A scenario for finite-time singularity in the quasigeostrophic model

Richard K. Scott†

School of Mathematics and Statistics, University of St Andrews, St Andrews KY16 9SS, Scotland, UK

A possible route to finite-time singularity in the quasigeostrophic system, via a cascade of filament instabilities of geometrically decreasing spatial and temporal scales, is investigated numerically using a high-resolution hybrid contour dynamical algorithm. A number of initial temperature distributions are considered, of varying degrees of continuity. In all cases, primary, secondary, and tertiary instabilities are apparent before the algorithm loses accuracy due to limitations of finite resolution. Filament instability is also shown to be potentially important in the closing saddle scenario investigated in many previous studies. The results do not provide a rigorous demonstration of finite-time singularity, but suggest avenues for further investigation.

Key words: geophysical and geological flows, instability

1. Introduction

The quasigeostrophic model is a leading-order approximation to the large-scale, low-frequency dynamics of the rotating, stratified flows of planetary atmospheres and oceans. In the presence of a horizontal boundary, such as the ground or ocean surface, it has long been recognized that the dominant motions are described by the dynamics at the surface itself, with interior dynamics playing a secondary role (Hoskins & Bretherton 1972; Blumen 1978). The same holds true at the rapid jump in static stability at the tropopause (Juckes 1994). In these cases the governing equations reduce to a single advection equation for the surface (potential) temperature θ, or surface buoyancy in the case of ocean dynamics:

$$\partial_t \theta + J(\psi, \theta) = 0, \quad \nabla^2 \psi = 0, \quad \theta = \psi_z, \tag{1.1}$$

where ψ is the horizontal streamfunction ($\boldsymbol{u} = (-\psi_y, \psi_x, 0)$), J is the Jacobian determinant, and ∇^2 is the three-dimensional Laplacian; the vertical coordinate has been rescaled by Prandtl's ratio, f/N, where f is the Coriolis parameter and N is the buoyancy frequency. The equations are often recast in purely two-dimensional form:

$$\partial_t \theta + J(\psi, \theta) = 0, \quad -(-\Delta)^{1/2} \psi = \theta, \tag{1.2}$$

where Δ is the two-dimensional Laplacian and the operator $(-\Delta)^{1/2}$ is most naturally defined in terms of the Fourier-transformed relation $\hat{\theta} = -|\boldsymbol{k}|\hat{\psi}$.

† Email address for correspondence: rks@mcs.st-and.ac.uk

Wider interest in the system (1.2) has arisen out of its similarity with the three-dimensional Euler equations. Taking the horizontal gradient of (1.2) yields an evolution equation for $\nabla\theta$ that bears strong similarity to the three-dimensional vorticity equation, in particular with regard to the structure of the stretching term $\nabla\theta \cdot \nabla\boldsymbol{u}$ (e.g. Constantin, Majda & Tabak 1994; Constantin 1995; Tran, Dritschel & Scott 2010). The similarity has motivated the investigation of the possible finite-time development of singularities from smooth initial conditions. Early numerical studies focusing on a closing saddle geometry suggested the possibility of singularity in finite time (e.g. Constantin *et al.* 1994), which was, however, later ruled out by higher-resolution studies, suggesting instead a double exponential growth $\nabla\theta \propto \exp\exp t$ (Ohkitani & Yamada 1997; Constantin, Nie & Schorghofer 1998). The later results were further supported by theoretical analysis, which showed, in particular, that if the closing saddle retains its simple form then no finite-time singularity is possible (Cordoba 1998).

Another possible route to singularity in the quasigeostrophic model was suggested by Hoyer & Sadourny (1982), involving the local transfer of enstrophy $\langle\theta^2\rangle$ to small scales through local instabilities. As argued by Pierrehumbert, Held & Swanson (1994) on dimensional grounds, since the growth rate of instabilities of small filaments of width d scales like $\sigma \sim \theta_0/d$, and since filaments are produced by ambient strain, which itself scales like σ, the evolution of d may be modelled by $\dot{d} \sim -\sigma d \sim -\theta_0$. Hence, d is linearly decreasing and filaments reach zero width in finite time. This local cascade is consistent with an early numerical simulation of Held *et al.* (1995) in which the roll-up of a straight filament generates a new filament, which in turn becomes unstable.

The purpose of this paper is to investigate the cascade through repeated filament instability and to consider (as far as possible with limited numerical resolution) the extent to which a self-similar cascade is achieved. If the repeated instabilities follow a self-similar pattern then, as discussed in §2 below, the development of a singularity in finite time appears inevitable. Establishing self-similarity is well beyond current computational limits. However, examining repeated instabilities for various initial filament profiles, as reported in §§3.1–3.3 below, provides some limited evidence that such a route to singularity may exist. We stress therefore that the results obtained so far are inconclusive but suggest that further investigation into this scenario is warranted.

Although the closing saddle scenario originally put forward by Constantin *et al.* (1994) was shown to lead to at most double exponential growth of $\nabla\theta$, instability of the collapsing θ ridge may again eventually dominate the stabilizing effect of background shear. That instability of the ridge was not previously observed appears to be due to the fact that the stabilizing effect of background shear is in this case particularly strong; instability does not become manifest until the ridge reaches widths that are well below the grid resolution of the earlier numerical investigations. The instability is illustrated here, again within the limits of current computational resources, in §3.4.

2. Properties of the filament instability

Before presenting some numerical examples, we first review the basic scaling for growth rates and outline the sense in which repeated instability may lead to finite-time singularity. The scenario, consisting of a discrete sequence of instabilities, is slightly
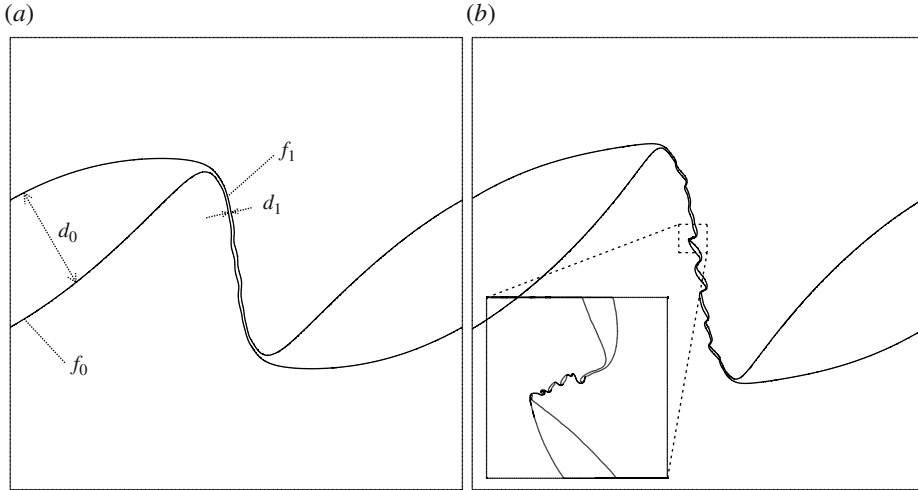
FIGURE 1. Snapshot of the strip boundary at (*a*) $t = 46$ and (*b*) $t = 46.8$ and magnification of central region. Initial boundary is at $y = \pm \pi/6 + 0.01 \sin x$; $\theta = 1$ inside the strip, $\theta = 0$ outside.

different from that described in Hoyer & Sadourny (1982), which focused on the continuous range of scales present in a fully developed turbulent flow.

For definiteness we consider an initially straight filament, f_0, with a cross-filament profile $\theta = f(y)$. On dimensional grounds, the growth rate of lateral perturbations $\eta(x)$ to the filament scales as θ_0/d_0, where θ_0 and d_0 are typical temperature and cross-filament length scales, respectively. The actual growth rate depends on the profile $f(y)$ but not sensitively (Juckes 1995; see also § 3.2 below). As perturbations grow, they saturate when $\eta \sim d$, at which point the original filament begins to roll up into elliptical patches connected by a new filament, f_1, similar to the filament instability of two-dimensional vortex dynamics (see figure 1*a*). The patches induce a background strain that has two effects: (i) it stretches the new filament f_1 causing the filament width to shrink exponentially (or possibly super-exponentially, as discussed below); and (ii) it provides a stabilizing effect on the new filament, similar to the two-dimensional case studied by Dritschel *et al.* (1991). The shrinking of the new filament f_1 implies that it will become unstable when the width, d_1 say, is such that the growth rate θ_0/d_1 sufficiently exceeds the background shear θ_0/d_0, which will occur on a time scale proportional to $\sigma_0^{-1} \sim d_0/\theta_0$. The secondary filament f_1 will therefore in turn roll up into a secondary instability, producing a tertiary filament f_2, etc.

Because of the inversion (1.2), interactions in this model are more local than for the case of two-dimensional vortex dynamics. As a result, to a good approximation the evolution of a given filament will be controlled purely by the influence of the parent filament that spawned it. At each stage, therefore, the new filament will become unstable when it shrinks to a certain fraction of the width of the parent filament; that is, we expect the ratio $d_i/d_{i-1} = \varepsilon$, where d_i is the width of the *i*th filament and where $\varepsilon \ll 1$, to remain independent of *i*. This being the case, the time taken for the *i*th filament to generate the $(i+1)$th filament is $\sigma_i^{-1} \sim d_i/\theta_0 \sim \varepsilon^i d_0/\theta_0$. The total time taken to generate the $(n+1)$th filament is $\sum_{i=0}^{n} \varepsilon^i d_0/\theta_0 \to (1 - \varepsilon)^{-1} d_0/\theta_0$ as $n \to \infty$. Hence a filament of zero width, and consequently infinite $\nabla \theta$, is produced in a finite time.

Although the time scale for the instability of a given filament is governed by the growth rate σ_i, the actual time taken to generate a new filament by roll-up will depend also on (i) the size of any initial perturbation and (ii) how it projects onto the scale of the fastest-growing unstable mode. Perturbations will exist in general because of the curvature of each filament near the elliptical patches of its parent. Let η_0 denote the size of the perturbation to the ith filament, relative to the width d_i, and, by locality, assume that it is independent of i. The evolution of η_0 may be divided into two phases: a primary phase of exponential growth of η_0 to order-one amplitude, followed by a secondary phase of exponential thinning of the new filament to the critical width for instability $d_{i+1} = \varepsilon d_i$. The total time taken is $\sim -\sigma_i^{-1} \log \eta_0 - \sigma_i^{-1} \log \varepsilon$. This factor may be large if η_0 is small or if ε is small, but if independent of i will only contribute a constant prefactor for the total time to generate the nth filament. Some caveats regarding the onset of the instability and the preservation of self-similarity will be discussed further in conjunction with the numerical illustrations and in § 4 below.

3. Numerical illustrations

We illustrate the possibility of self-similar instabilities in four simple contexts: the first three, filaments with different initial cross-sectional θ profiles; the last, the closing saddle flow mentioned in the introduction and examined extensively in previous studies. All cases suggest the possibility of a cascade of instabilities, although it must be stressed that current numerical resolution is insufficient to yield a definitive demonstration of a self-similar singularity. Because the ratio ε tends to be extremely small, we are unable to follow the evolution beyond the second or third instability. Further, self-similarity in the cross-sectional θ profiles is definitely not preserved in the distributed filament profiles considered in §§ 3.2 and 3.3.

3.1. *Strip*

The simplest profile comprises a strip of uniform θ:

$$\theta_0(y) = \begin{cases} 1 & |y| \leqslant d, \\ 0 & \text{otherwise,} \end{cases} \tag{3.1}$$

which has the advantage that the form of the profile is trivially maintained at all stages of the evolution. Because the initial profile is discontinuous, however, the sense in which finite-time singularity is meant requires modification. In fact, not only is the initial $\nabla \theta$ already singular, but there is also a logarithmic singularity in the along-strip velocity at $y = \pm d$ (Juckes 1995). From a Lagrangian perspective the singularity is removable: it is tangent to the filament boundary and so does not contribute to the evolution of the boundary, which may be described by a smooth map. One sense in which singularity formation may thus be considered is as a change in the topology of the strip due to the shrinking to zero of the distance between opposite sides of the strip at some point. A similar problem of singularity formation from the interaction of two interacting patch distributions of θ was considered recently by Cordoba *et al.* (2005).

The instability cascade is illustrated in figure 1, which shows snapshots of the filament boundary for a strip of strength $\theta = 1$, half-width $d = \pi/6$, solved in a $2\pi \times 2\pi$ doubly periodic domain with a hybrid contour-dynamical method described in the Appendix. The initial strip is perturbed by displacing the contours by a distance $\eta_0 = 0.01 \sin x$. At $t = 46$ the secondary filament generated by the initial instability begins to roll up into a secondary instability. Very soon afterward, the
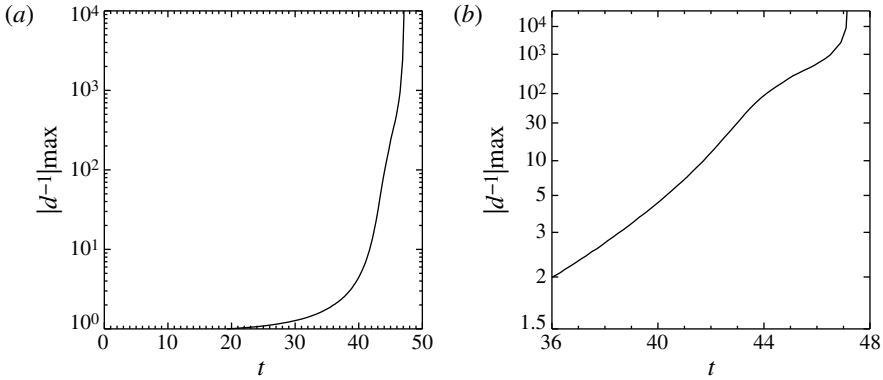
FIGURE 2. Inverse minimum cross-filament distance against time on a log–linear scale (*a*)
and loglog–linear scale (*b*).

secondary instability itself can be seen to generate tertiary filaments which in turn
become unstable. The collapse in spatial and temporal scales at each stage is evident:
the second instability develops over a time interval $\Delta t \sim O(1)$; the third instability
develops over an interval $\Delta t \sim O(0.1)$ (inset). At this point the numerical scheme is no
longer able to accurately follow the evolution.

The increase of the inverse minimum cross-filament distance in time is shown in
figure 2. A period of initially super-exponential growth, up to around $t = 43$, in line
with that found by Ohkitani & Yamada (1997) and Constantin *et al.* (1998) for the
closing saddle, and suggesting that this growth may be typical for this system, appears
to saturate before the onset of the secondary instability. The secondary instability at
$t = 46$ shows a much more rapid increase in growth, although the short time range
available here makes a definite fit difficult.

Another indication of the possibility of finite-time singularity is given by the energy
dissipation. In the viscous system (with a viscous term $\nu \Delta \theta$ on the right-hand side
of (1.2)), a condition for finite-time singularity is that the instantaneous maximum, or
peak, energy dissipation, $\varepsilon_T \to C > 0$ as the viscosity $\nu \to 0$. The present numerical
scheme dissipates only through discretization errors of the finite grid, but we may
consider the dependence of the dissipation on the grid resolution, shown in figure 3 for
inversion grid resolutions $N = 512, 1024, 2048, 4096$ (θ is accurately represented on a
grid four times finer), with increasing grid resolution corresponding to decreasing ν.
The peak dissipation ε_T occurs around the onset of the secondary and tertiary
instabilities and is remarkably uniform across the four cases.

3.2. *Smoothed strip*

To avoid the singularity associated with the discontinuous initial θ profile, we consider
next a smooth profile by convolving the strip with a Gaussian kernel. Following Juckes
(1995), we define

$$\tilde{\theta}_0(y) = \frac{1}{\sqrt{2\pi\delta}} \int \theta_0(y') e^{(y-y')^2 / 2\delta} \, \mathrm{d}y' \tag{3.2}$$

with $\theta_0(y)$ given by (3.1) and where δ is a parameter controlling the transition from
$\theta = 0$ outside to $\theta = 1$ inside the strip. Juckes (1995) demonstrated that for values of
$\delta \lesssim 0.4$ the growth rate of the linear instability and wavenumber of the maximum
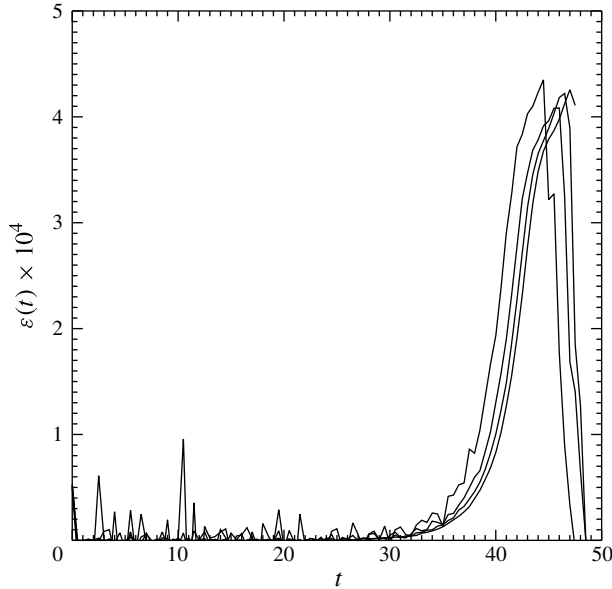
FIGURE 3. Evolution of the energy dissipation $\varepsilon(t)$, calculated directly from the total energy, for inversion grid resolution $N = 512, 1024, 2048, 4096$ (peaks moving left to right).
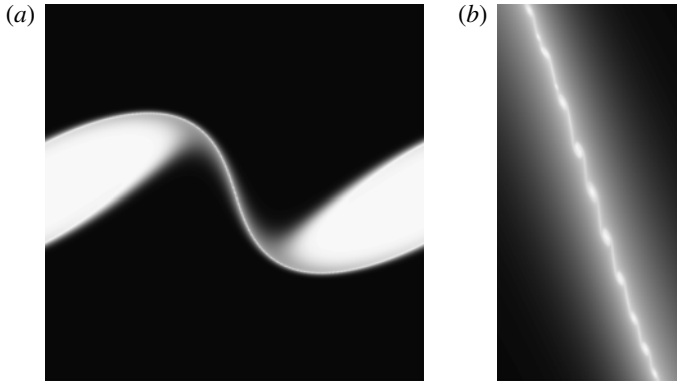

FIGURE 4. θ field at time $t = 40$ for the strip smoothed according to (3.2) with $\delta = 0.1$; full field (*a*) and $8\times$ magnification of the central region (*b*).

growing mode remain close to those of the strip (see Juckes (1995), figure 1). In the numerical method used here, the smooth profile is represented by contours of constant θ at increments $\Delta\theta = 0.01$. The instability is again initiated by a y-displacement of each contour by an amount $0.01 \sin x$.

Figure 4 shows a snapshot of the θ field at $t = 40$, including an $8\times$ magnification of the central region. The secondary instability is again apparent in the enlargement, although its scale is markedly smaller than in the case of the strip, both in the along-filament wavelength and the cross-filament extent. The filament has here been stretched to a smaller width before the onset of the secondary instability.
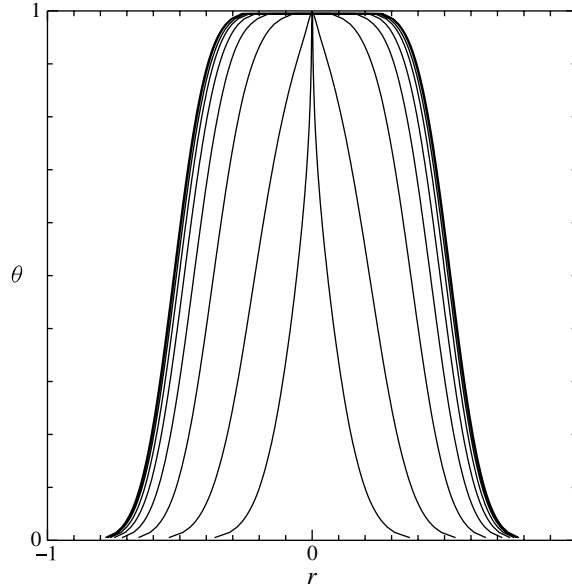
FIGURE 5. Cross-sections of the θ profile along a line through the origin and normal to the filament centre, at times $t = 0, 5, 10, \ldots, 35$ and $t = 39$ (outer lines to inner).

The reduction in scale is associated with the time evolution of the filament cross-section. Figure 5 shows cross-sections of the filament along a line through the origin and normal to the filament maximum at times from $t = 0$ to $t = 39$, just before the onset of the secondary instability. It is clear that the filament does not preserve its initial profile during the evolution of the primary instability and the formation of the secondary filament. A large skirt of low θ values is left at relatively large distances from the filament centre while the θ values near the centre exhibit more rapid compression, leading to a sharply peaked ridge. The secondary instability shown in figure 4 involves primarily these large θ values near the filament centre while the skirt initially remains laminar. The relative magnitude of the θ values involved in the secondary instability relative to the background skirt is therefore less than for the primary instability. It is not clear whether this decrease in effective filament strength will be offset at all stages of instability by the shrinking filament width, such that the filament instability remains sufficiently vigorous to overcome the stabilizing effect of the ambient shear. Hints of tertiary instability may be seen in places, but at these scales numerical resolution is clearly inadequate.

3.3. *Elliptical cross-section*

We consider next a case in some regards intermediate between the strip and smoothed strip profiles discussed above. We define the initial cross-section by the function

$$\theta(y) = (1 - y^2/d^2)^{1/2}, \tag{3.3}$$

belonging to a class of elliptical θ distributions discussed in Dritschel (2011). The profile is continuous and, although there is a weak singularity in $\nabla\theta$ at $y = \pm d$, the velocity field is everywhere regular. For a horizontally elliptical patch (as opposed to a filament), Dritschel (2011) showed that the elliptical cross-section gives an exact uniformly precessing solution to (1.2), stable for horizontal aspect ratios $\gtrsim 0.427$.
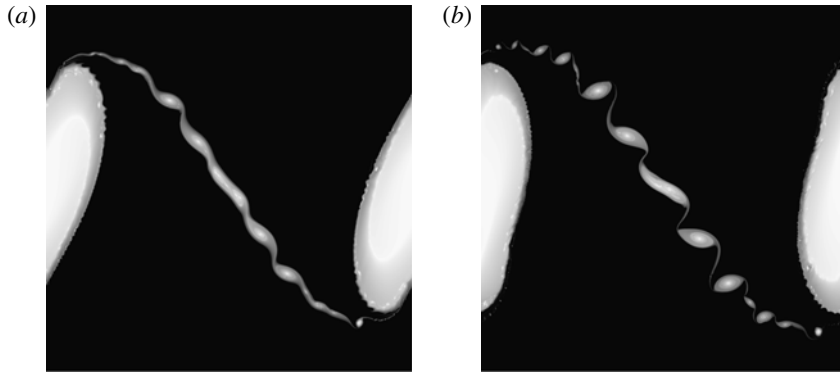
FIGURE 6. The θ field at $t = 42$ (*a*) and $t = 43$ (*b*) from the initial profile (3.3).

The evolution of the filament during the initial instability is similar to that of the smooth strip discussed above: in particular, the filament cross-section develops a strongly peaked structure similar to that shown in figure 5. Thus, the secondary instability again involves initially only θ values from near the centre of the strip. The arguments of §2 may still, however, be applied, by considering the distance between the two outermost contours $\mathscr{C}_0^{\pm}$ defining the profile (initially at $y = \pm d$). Suppose that the secondary, tertiary, etc., instabilities in the filament core do not lead to a finite-time singularity, but rather serve simply to partially homogenize θ between $\mathscr{C}_0^{\pm}$. Rapid shrinking of the distance between $\mathscr{C}_0^{\pm}$ will still lead to a situation in which the filament bounded by those contours becomes sufficiently unstable to overcome the effect of ambient shear. The arguments of §2 again suggest a series of instabilities of the entire filament as defined by $\mathscr{C}_0^{\pm}$, leading to a collapse in the minimum separation between the two contours. In this case, the fact that there exists a material line lying between $\mathscr{C}_0^{\pm}$ on which $\theta = 1$ implies that a jump discontinuity in θ would develop in finite time from the initially continuous profile.

Figure 6 shows two snapshots of the θ field arising from this initial condition, illustrating the above scenario. Although the secondary instability of the filament core began around $t = 36$, we ignore it and the possibility of singularity formation in the filament core. Continuing the time integration (increased numerical dissipation was necessary to regularize the complex θ field emerging in the core), we find that between $t = 42$ and $t = 43$ the filament as defined by $\mathscr{C}_0^{\pm}$ becomes unstable. The secondary instability of $\mathscr{C}_0^{\pm}$ leads to further rapid collapse of the distance between these contours and evidence of tertiary instability is again visible.

3.4. *The closing saddle*

Finally, we revisit briefly the initial condition considered originally by Constantin *et al.* (1994). In more recent studies of this flow (Ohkitani & Yamada 1997; Constantin *et al.* 1998), it was concluded that the maximum $|\nabla\theta|$ grows like $\exp\exp t$, with possible decrease in the growth at later times. This has been confirmed by the present calculations up until time $t = 8.9$. Here, we conclude that until this time the large-scale shear flow due to the large-scale θ distribution is sufficient to stabilize any filament instability. At $t = 8.9$, however, the filament has shrunk to an extent that the instability is no longer suppressed and it again rolls up, generating narrower filaments on a shorter time scale (figure 7). That this instability was not apparent in earlier studies is most likely due to limited resolution; with a pseudo-spectral model at 4096^2 resolution
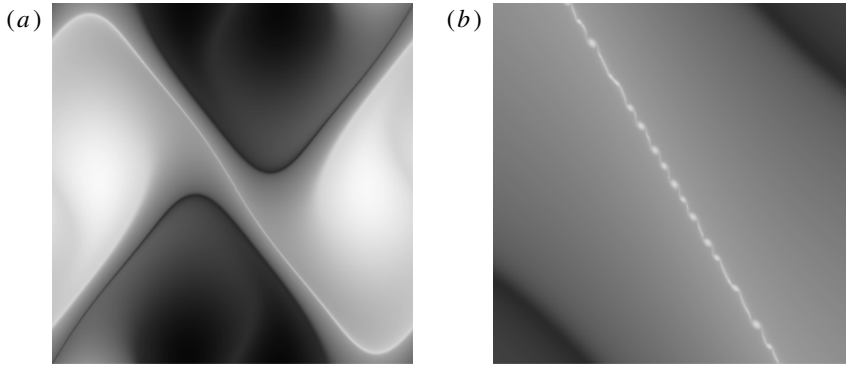
FIGURE 7. The θ field from the initial condition $\theta = \cos y - \sin x \sin y$ at $t = 8.9$ (*a*) and a $16\times$ magnification of the origin at $t = 9.1$ (*b*).

it is possible to follow the inviscid evolution only until just beyond $t = 8$. In the present case, the contoured θ field is retained on a fine-grid of $32\,786^2$ and dissipation occurs at scales strictly below this grid scale.

4. Discussion

The possibility of finite-time singularity formation in the quasigeostrophic model, via a self-similar cascade of scales, was suggested previously by Hoyer & Sadourny (1982) and Pierrehumbert *et al.* (1994). In this paper, we have provided some limited numerical support for this scenario using high-resolution, hybrid contour dynamical numerical simulations starting from a variety of initial conditions. In all cases the tendency for filaments to roll up in such a way as to produce new, narrower filaments that also roll up, on a shorter time scale, is evident and robust. A finite-time singularity appears plausible, though subject to the following important caveats.

(*a*) Numerical resolution, though relatively high, is insufficient to follow the cascade beyond the second or third instability. By the third instability accurate computation of quantities such as $\nabla\theta$ is no longer possible.

(*b*) In the cases of distributed θ profiles, the filament cross-section does not retain its initial profile and so self-similarity of the instabilities is not preserved. This may have only a modifying effect on the cascade in the case of the elliptical cross-section (§ 3.3). In other cases it may eventually weaken the difference in θ values between the filament core and its most immediate surroundings such that subsequent instabilities are suppressed.

(*c*) As described in § 2, any arbitrary small perturbation to the filament, such as arising from curvature in the mean flow, is sufficient to realize the cascade. This argument may fail, however, if in regions where the filament is thinning fastest it is also straightening to such an extent that perturbations are in effect excluded from the most unstable region. Figure 3 indicates that at lower resolutions the secondary instability is triggered earlier, suggesting the possible role of numerical errors, although the time of onset does appear to converge with increasing resolution. A similar series of experiments for the case of the closing saddle also indicates a slight delay in the onset of the instability with increasing resolution. Whether the onset of the instability indeed converges to a finite time at ever higher resolution will need to await more powerful numerical calculations.

In summary, the rapid increase of growth rate associated with the collapsing filament makes a cascade of instabilities a plausible scenario, and the current work is illustrative of how this might lead to finite-time singularity. It is hoped that future work making use of more sophisticated, adaptive grid numerical schemes will address the above caveats in more detail and provide further support for the presence or absence of such a singularity.

Appendix

The numerical algorithm used to integrate (1.2) is an adaptation of the contour advective, semi-Lagrangian algorithm developed by Dritschel & Ambaum (1997). The efficiency of this method in representing two-dimensional freely decaying turbulence was recently demonstrated by Dritschel & Scott (2009). The only modification required here is to the Green's function relating the active scale to the streamfunction. The more local nature of the Green's function in the present case means that a fine underlying grid is required to accurately represent the velocity field, which retains significant power at small scales (see also Dritschel 2011).

For the experiment described in §3.1 a single contour defines each edge of the strip. At each time step the θ field is gridded onto a $16\,384^2$ grid before averaging onto a 4096^2 grid and inverting to give ψ. Each contour is represented by a sequence of nodes, whose density increases with increasing curvature to accurately represent each contour (Dritschel 1989). Contour surgery, used to control the growth in nodes, is effective on scales below that of the finest grid.

For the experiments involving distributed profiles (§§3.2–3.4), the smooth θ field is represented by contours at intervals of $\Delta\theta = 0.01$. A few experiments carried out with $\Delta\theta = 0.005$ showed no significant differences from those reported here. In §§3.2 and 3.3, the fine grid resolution is again $16\,384^2$; for the closing saddle experiment described in §3.4, it is $32\,768^2$.

REFERENCES

BLUMEN, W. 1978 Uniform potential vorticity flow. Part I. Theory of wave interactions and two-dimensional turbulence. *J. Atmos. Sci.* **35**, 774–783.

CONSTANTIN, P. 1995 Nonlinear inviscid incompressible dynamics. *Physica D* **86**, 212–219.

CONSTANTIN, P., MAJDA, A. J. & TABAK, E. 1994 Formation of strong fronts in the 2D quasigeostrophic thermal active scalar. *Nonlinearity* **7**, 1495–1533.

CONSTANTIN, P., NIE, Q. & SCHORGHOFER, N. 1998 Nonsingular surface quasi-geostrophic flow. *Phys. Lett.* A **241**, 168–172.

CORDOBA, D. 1998 Nonexistence of simple hyperbolic blow-up for the quasi-geostrophic equation. *Ann. Math.* **148**, 1135–1152.

CORDOBA, D., FONTELOS, M. A., MANCHO, A. M. & RODRIGO, J. L. 2005 Evidence of singularities for a family of contour dynamics equations. *Proc. Natl Acad. Sci.* **102**, 5949–5952.

DRITSCHEL, D. G. 1989 Contour dynamics and contour surgery: numerical algorithms for extended, high-resolution modelling of vortex dynamics in two-dimensional, inviscid, incompressible flows. *Comput. Phys. Rep.* **10**, 78–146.

DRITSCHEL, D. G. 2011 An exact steadily rotating surface quasi-geostrophic elliptical vortex. *Geophys. Astrophys. Fluid Dyn.* **105**, 368–376.

DRITSCHEL, D. G. & AMBAUM, M. H. P. 1997 A contour-advective semi-Lagrangian numerical algorithm for simulating fine-scale conservative dynamical fields. *Q. J. R. Meteorol. Soc.* **123**, 1097–1130.

DRITSCHEL, D. G., HAYNES, P. H., JUCKES, M. N. & SHEPHERD, T. G. 1991 The stability of a two-dimensional vorticity filament under uniform strain. *J. Fluid Mech.* **230**, 647–665.

DRITSCHEL, D. G. & SCOTT, R. K. 2009 On the simulation of nearly inviscid two-dimensional turbulence. *J. Comput. Phys.* **228**, 2707–2711.

HELD, I. M., PIERREHUMBERT, R. T., GARNER, S. T. & SWANSON, K. L. 1995 Surface quasi-geostrophic dynamics. *J. Fluid Mech.* **282**, 1–20.

HOSKINS, B. J. & BRETHERTON, F. P. 1972 Atmospheric frontogenesis models: mathematical formulation and solution. *J. Atmos. Sci.* **29**, 11–37.

HOYER, J.-M. & SADOURNY, R. 1982 Closure modelling of fully developed baroclinic instability. *J. Atmos. Sci.* **39**, 707–721.

JUCKES, M. N. 1994 Quasigeostrophic dynamics of the tropopause. *J. Atmos. Sci.* **51**, 2756–2779.

JUCKES, M. N. 1995 Instability of surface and upper-tropospheric shear lines. *J. Atmos. Sci.* **52**, 3247–3262.

OHKITANI, K. & YAMADA, M. 1997 Inviscid and inviscid-limit behaviour of surface quasigeostrophic flow. *Phys. Fluids* **9**, 876–882.

PIERREHUMBERT, R. T., HELD, I. M. & SWANSON, K. L. 1994 Spectra of local and nonlocal two-dimensional turbulence. *Chaos, Solitons Fractals* **4**, 1111–1116.

TRAN, C. V., DRITSCHEL, D. G. & SCOTT, R. K. 2010 Effective degrees of nonlinearity in a family of generalized models of two-dimensional turbulence. *Phys. Rev.* E **81**, 01630.